ISSN 1063-780X, Plasma Physics Reports, 2010, Vol. 36, No. 3, pp. 271–278. © Pleiades Publishing, Ltd., 2010.

LOW-TEMPERATURE PLASMA

Double Layer in a Cylindrical Hollow-Cathode Discharge[1]

A. Abu-Hashem[a], M. A. Abd Al-Halim[a, b], M. A. Hassouba[a], and M. M. Masoud[c]

[a] *Benha University, Benha, Egypt*

[b] *North Carolina State University, Raleigh, USA*

e-mail: ma_halim74@yahoo.com

[c] *Nuclear Research Center, Atomic Energy Authority, Cairo, Egypt*

Received February 18, 2009; in final form, May 12, 2009

Abstract—A dc cylindrical coaxial glow discharge with an inner grid anode has been studied. The region between the two electrodes is seen dark, while a brightly glowing region forms inside the grid anode up to the center. The current-voltage characteristic of a dc cylindrical glow discharge in nitrogen is similar to that of a normal glow discharge, while the normal glow discharge voltage decreases with increasing pressure. The minimum plasma potentials are observed in the hollow cathode region due to the accumulation of electrons at the back of the grid anode. At the center, some of the passed electrons are converged, so their potential is decreased. These electrons have a sufficient time to be redistributed to form one group with a Maxwellian electron energy distribution function. The electron temperature measured by electric probes varies from 1.6 to 3.6 eV, while the plasma density varies from 3.9×10^{16} to 7×10^{13} m^{-3}, depending on the discharge current and probe position. The plasma density increases as the electrons move radially from the grid toward the central region, while their temperature decreases.

DOI: 10.1134/S1063780X10030098

1. INTRODUCTION

The cylindrical glow discharge consists of two coaxial cylindrical electrodes. The aim of the cylindrical or spherical structure, with grid anode, is to provide inertial electrostatic confinement of electrons [1]. When the outer electrode is the cathode and the inner grid electrode is the anode and a suitable voltage is used to operate the system, gas breakdown occurs and the negative glow region forms at the center of the grid anode. The electrons are rapidly emitted and accelerated from the cathode toward the grid anode. The electron beam passes through the anode and is injected toward the grid center. When the beam current is higher than the space-charge-limited current of this area, these electrons will be confined at the center of the spherical or cylindrical grid anode, causing the so-called "cathode." In addition, under proper conditions, the ion and electron flows create a space-charge-induced "double potential" well (a negative and a positive potential well) [2]. This structure traps high-energy electrons at the center of the inner electrode.

The coaxial virtual cathode oscillator consists of two metallic coaxial cylindrical electrodes. The inner electrode is positively biased grid, while the outer electrode is negatively biased discharge vessel. It has been shown that the forward current increases significantly as the gap distance between the cathode and the anode increases [3].

Rozsa et al. [4, 5] investigated laser oscillation on Al II transitions in a large-diameter hollow cathode discharge tube, where Al vapor was produced by cathode sputtering. A special internal anode system considerably increased the tube voltage, which resulted in a low threshold current and an increased output power [4]. This effect was also observed on the 469.4 nm Kr and the 476.5 nm Ar ion transitions. A continuous-wave laser oscillation was observed for the first time on the 531.4 and 486.3 nm transitions of Xe II [5]. A higher voltage is required to increase the rate of volumetric ionization, thereby compensating ion loss by diffusion from the negative glow. The focusing of fast electrons toward the tube axis increased laser excitation in this region. Strong laser action with a low threshold current was achieved on the 283-nm Au II transition [6]. The threshold current was 0.4 A for the strongest 780.8 nm laser line near IR transitions of Cu II. At a discharge current of 2.4, a multiline output power of 30 mW was obtained on six transitions between 740.4 and 789.6 nm [7].

Iijima [8] studied a high-voltage hollow cathode discharge tube with an internal helical anode as an excitation source of metal vapor lasers. He found that the intensity ratio of the HeII to HeI lines emitted from this hollow cathode tube increased with increasing operating voltage, which in turn increased with increasing axial magnetic field. The radial distribution of the emitted luminous intensity is symmetric with respect to the axis. The current–voltage (I–V) charac-

[1] The article is published in the original.

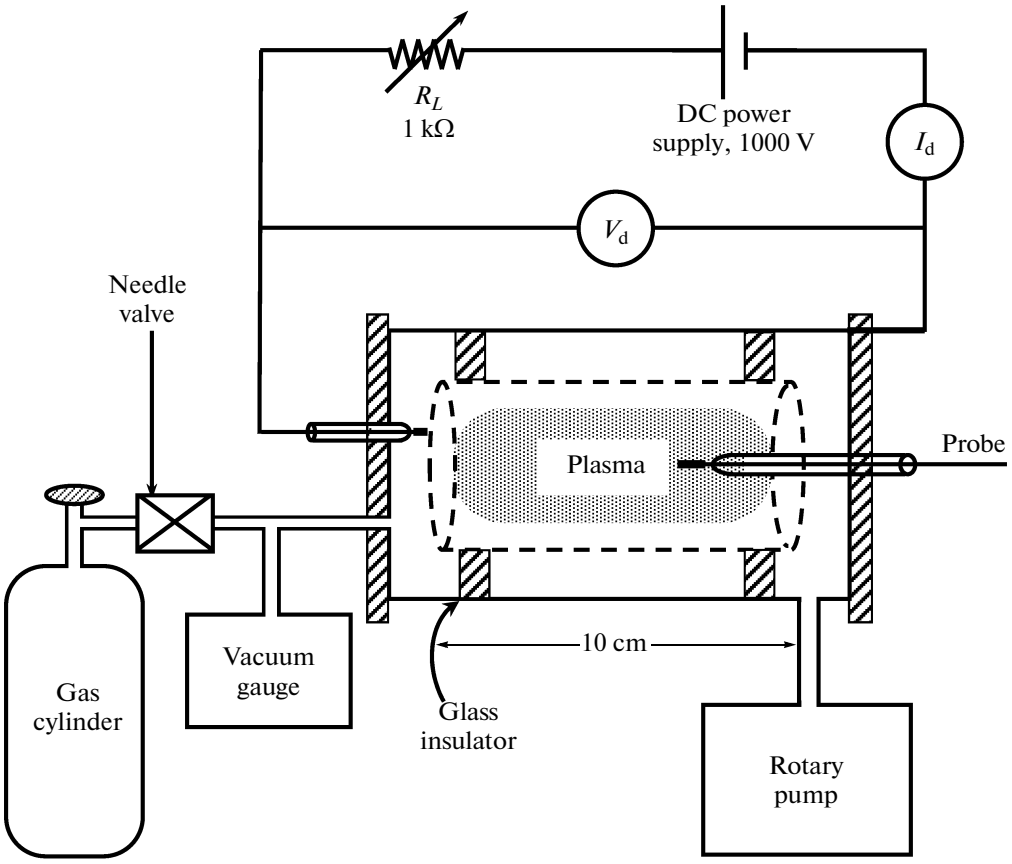

Fig. 1. Schematic diagram of the experiment.

teristic was controlled by changing the distance between the threads of the helical anode [9].

Fujii studied the confining process which attracts a negative glow within a hollow cathode of cylindrical geometry. The confining was interpreted as a transition process from a Townsend discharge to a normal glow discharge. The efficiency of the laser tube increases as the product *Pd* (the pressure multiplied by the interelectrode distance) decreases and also as the hole diameter of the cathode wall approaches the inner diameter of the hollow cathode [10].

The discharge characteristics were discussed morphologically with a view to applying this tube to a metal vapor laser [11]. In the negative glow of a low-pressure He and a He–Cd discharge, some electrons have energies more than 100 eV and the density of low-energy (30–34 eV) electrons is twice as high as that in the positive column [12]. It was found that a hollow-cathode metal ion lasers provided more than twenty wavelengths with a significant output. They measured the density of sputtered metal atoms as a function of the discharge current and gas pressure. Excitation of the upper laser levels occurred via charge transfer reaction, and the required ground state metal density was generated via sputtering [13].

The aim of present work is to operate a dc cylindrical glow discharge with coaxial electrodes, where the inner grid anode is a grid, which forms a negative layer inside the real grid anode using nitrogen gas. The electrical characteristics and the plasma parameters (the plasma potential, electron temperature T_e, plasma density N, and electron energy distribution function (EEDF)), which vary radially from the grid anode toward the center of the grid, are determined.

2. EXPERIMENTAL SETUP

A schematic diagram of the experimental setup is shown in Fig. 1. The discharge vessel is a cylindrical stainless-steel tube 15 cm in length and 5 cm in diameter. A 10-cm-long 4-cm-diameter high-transparency stainless-steel cylindrical grid is enclosed inside the discharge vessel. The two cylinders are hollow and coaxial. The outer cylinder (discharge vessel) and the inner grid cylinder represent the cathode and the anode, respectively. The two cylindrical electrodes are insulated from one another by two glass discs.

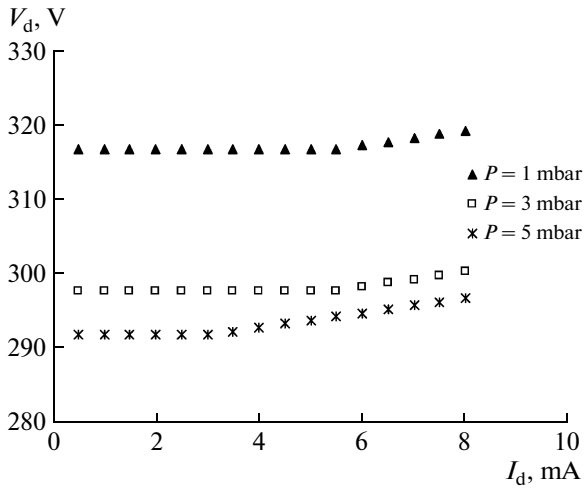

Fig. 2. I–V characteristic of a cylindrical hollow-cathode discharge at different nitrogen pressures.

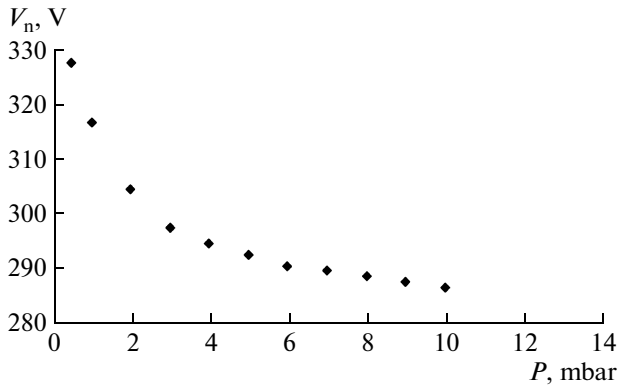

Fig. 3. Relation between the normal glow voltage as a function of the nitrogen pressure.

The discharge vessel is evacuated and filled with nitrogen, and the pressure is controlled by dynamic continuous flow. The distance between the two electrodes is fixed at 0.5 cm. The discharge vessel has three side ports: the first port is used for the working nitrogen gas flow from the gas cylinder through a needle valve, the second one is used to insert an electric probe (single or double) inside the plasma, and the third one is connected to the vacuum system.

A single Langmuir probe is used to measure the plasma potential, the electron temperature, and the plasma density and estimate the EEDF. The single probe is made of a tungsten wire with a radius of 0.14 mm and length of 3 mm. Also, a double electric probe is used to estimate the electron temperature and plasma density. It consists of two tungsten wires, each had a radius of 0.14 mm and length of 2 mm, which are separated from one another by a distance of 2 mm. Both the single and double probes were fitted inside the inner grid electrode.

3. RESULTS AND DISCUSSION

In the present work, a dc cylindrical coaxial glow discharge with an inner grid anode is studied using nitrogen as a working gas. When breakdown occurs between the two coaxial electrodes, the region between them is seen dark, while a brightly glowing region forms inside the grid anode up to the center. In this paper, we consider the I–V characteristic, the radial distributions of the potential and electric field, the EEDF, the electron temperature, and the plasma density.

3.1. The Current-Voltage Characteristic of the Discharge

The I–V characteristic of a dc cylindrical glow discharge in nitrogen was measured. Figure 2 shows the I–V characteristics of the discharge at nitrogen pressures of 1, 3, and 5 mbar. At a nearly constant discharge voltage V_d, the discharge current increases with pressure. These curves are similar to that of a normal glow discharge [14, 15, 16]. The figure also shows that the discharge voltage increases with decreasing gas pressure at a constant discharge current. Since, at low gas pressures, collisions between electrons and gas atoms decrease and, thus, the mean free path increases, large values of the discharge voltage will be required to maintain the discharge [17].

Figure 3 shows the relation between the normal glow discharge voltage V_n (the voltage at which the normal glow region starts) as a function of the gas pressure. It is found that the normal glow discharge voltage V_n decreases sharply in the pressure range 0.5–3 mbar and decreases slowly at higher pressures. The decrease in the normal glow discharge voltage V_n with increasing gas pressure can be explained according to the relation between V_n and the secondary ionization coefficient (ω/α) as [18]

$$V_n = \frac{1}{\eta}\ln\left[1+\left(\frac{1}{\omega/\alpha}\right)\right], \quad (1)$$

where η is the average number of ion pairs per volt produced by an electron and ω/α is the generalized secondary ionization coefficient. It is clear from Eq. (1) that the normal glow voltage V_n decreases with increasing ω/α. It is well known that ω/α depends on the type of secondary processes active in the discharge. If these processes are photoelectric and/or excited atoms processes, then electron emission from the cathode rises. This means that ω/α certainly depends on the gas pressure. As the gas pressure increases, the

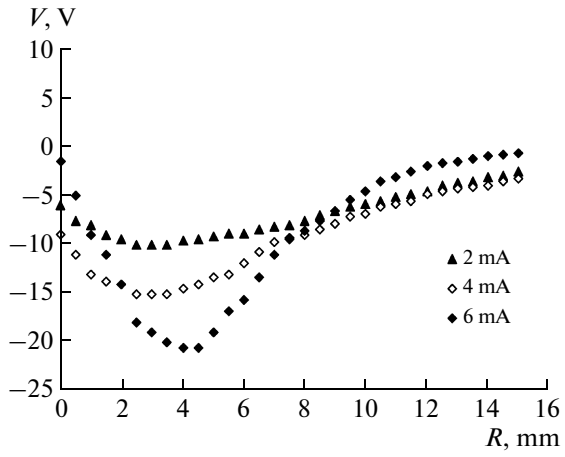

Fig. 4. Radial distribution of the electrostatic potential inside the cylindrical hollow-cathode system at a constant nitrogen pressure of 3 mbar for different discharge currents.

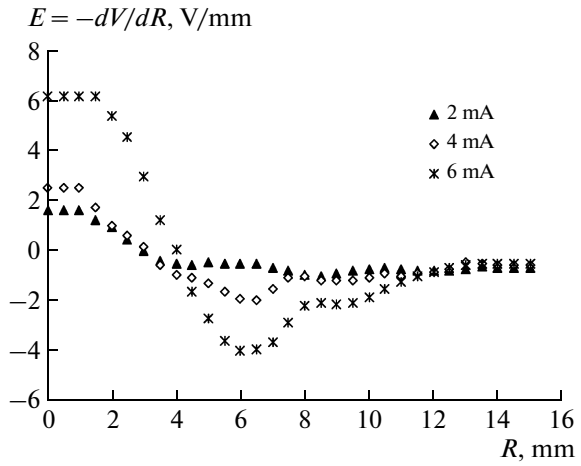

Fig. 5. Radial distribution of the electric field inside the cylindrical hollow-cathode system at a constant nitrogen pressure of 3 mbar for different discharge currents.

ratio ω/α increases; hence, according to Eq. (1), V_n should decrease [19]. This is similar to the left-hand side of the Paschen curve [14].

3.2. Radial Distribution of the Potential and Electric Field

The plasma potential V_s is an important parameter that is used to determine the electron saturation current I_{es} from the I–V curve of the single probe. The plasma potential can be determined from the zero-crossing point of the second derivative of the I–V characteristic of the single probe [20, 21]. The single probe is fitted inside the inner grid anode and moved radially away from the grid anode ($R = 20$ mm) toward the center ($R = 0$ mm). Figure 4 shows the plasma potential distribution as a function of the radial position for a nitrogen discharge at a pressure of 3 mbar and discharge currents of 2, 4, and 6 mA.

When an electron beam is accelerated in the interelectrode gap, it passes through the anode grid and is injected into the area located on the other side of the anode. When the beam current is higher than the space-charge-limited current in this area, a region with a high electron density forms at a certain position that reflects a fraction of electrons, depending on the electron energy. The plasma has a negative potential because of the excess number of electrons that are accumulated in the inner region. The minimum peaks in Fig. 4 form at radial positions of 2.5, 3, and 4 mm from the center at discharge currents of 2, 4, and 6 mA, respectively.

In the right part of Fig. 4, the space charge of the electron beam generates an electric field that decelerates electrons to arrive at the center. When this effect is strong enough, some electrons are reflected by the electric field of the beam. As the electrons move radially from the grid anode toward the center, their kinetic energy decreases, while their potential increases. In the left part of Fig. 4, some of the passed electrons from the negative layer formed at the back side of the anode grid are converged toward the center ($R = 0$ mm). The kinetic energy of these electrons increases, whereas their potential decreases.

The radial distribution of the electric field obtained from the potential distribution using the relation $E = -dV/dR$ is shown in Fig. 5. It is seen that the electric field is weak near the grid anode. As the electrons move toward the center, the electric field decreases (increases in the negative direction) until reaching the front of the negative layer region, in which the electric field increases (decreases in negative direction) to become zero.

After that, the electric field changes its sign and increased as the electrons move till reaching the center. This behavior can be explained according to the trapping process. After breakdown occurs, a uniform electron beam is injected and moves rapidly toward the grid anode. A large number of electrons near the grid leads to a weak electric field in this region. The electron beam passes through the grid anode making a large number of ionizing collisions with neutral gas atoms. This leads to the production of secondary electrons, which loss most of their energy also in collisions with gas atoms; most of them are found to be trapped. These trapped electrons determine the plasma density, but do not contribute to the electron current [22]. These trapped electrons produce a reversal field, so the electric field is decreased till reaching the negative layer. When the electron beam current is higher than the space-charge-limited current of the area behind the grid anode, a high electron density is accumulated [23]. The accumulated electrons decelerate a certain

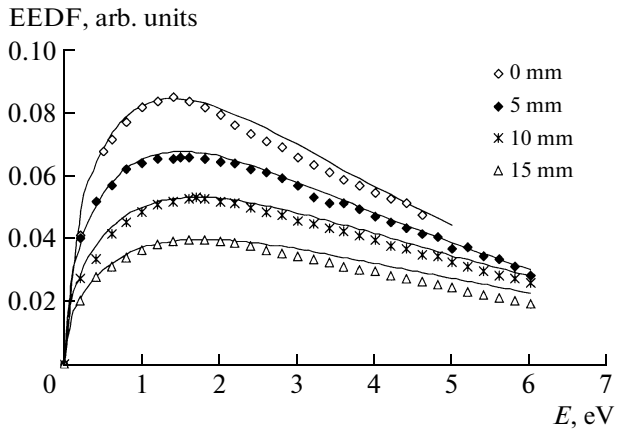

Fig. 6. Comparison of Maxwellian distributions with the experimental EEDFs at different radial positions for a constant discharge current of 6 mA and constant nitrogen pressure of 3 mbar. The symbols show the experimental results, while the solid lines represent Maxwellian distributions.

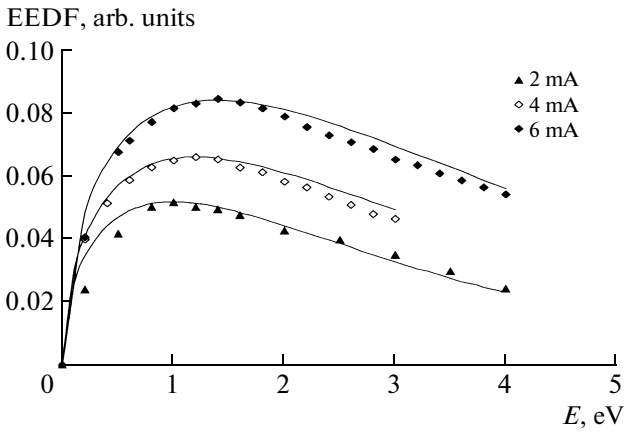

Fig. 7. Comparison of Maxwellian distributions with the experimental EEDFs at the center of the system ($R = 0$) for a constant nitrogen pressure of 3 mbar and different discharge currents. The symbols show the experimental results, while the solid lines represent Maxwellian distributions.

part of the electron beam; this means that the number of electrons that pass through region occupied by the converged electrons decreases, so the electric field in that region increases.

3.3. Determination of the EEDF

Knowing the EEDF helps to explain mechanisms of the glow discharge in different regions. In most plasma diagnostics, the EEDF is usually assumed to be Maxwellian. This assumption is valid only for the case where charged particles are in equilibrium with neutral gas atoms [24]. The method that gives the EEDF is based on measuring the second derivative of the electron probe current with respect to the probe potential (d^2I_e/dV^2) [25].

The EEDF can be obtained using the second derivative of the electron probe current, according to the following relation [24, 26]:

$$F(E) = \frac{4}{A_\mathrm{p} e^2}\sqrt{\frac{mV_\mathrm{p}}{2e}}\frac{d^2I_e}{dV_\mathrm{p}^2}, \qquad (2)$$

where m is the electron mass and A_p is the probe surface area.

Numerical differentiation of the single-probe curves was carried out by a computer program to obtain the first and second derivatives of the electron probe current with respect to the probe potential (dI_e/dV_p and d^2I_e/dV_p^2). Then, the second derivative was multiplied by $V_\mathrm{p}^{1/2}$ and plotted with the probe potential V_p to obtain the EEDF.

For a Maxwellian EEDF, the following relation is valid [27]:

$$\frac{d^2I_e}{dV_\mathrm{p}^2} \propto \exp\left(-\frac{eV_\mathrm{p}}{kT_e}\right), \qquad (3)$$

where k is the Boltzman constant and T_e is the electron temperature. Thus, the Maxwellian EEDF is given by [27]

$$F(E) = \mathrm{const} \times \sqrt{V_\mathrm{p}}\exp\left(-\frac{eV_\mathrm{p}}{kT_e}\right). \qquad (4)$$

The theoretical Maxwellian distribution is obtained by calculating the Maxwellian EEDF from Eq. (4) and comparing it with the experimental results.

Figure 6 compares the Maxwellian distribution with the experimental EEDF measured at different radial positions (0, 5, 10, and 15 mm) at a discharge current of 6 mA and gas pressure of 3 mbar, while Fig. 7 compares the Maxwellian distribution with the experimental EEDF measured at different discharge currents (2, 4, and 6 mA) at the center of the system ($R = 0$ mm) at a gas pressure of 3 mbar.

It is seen from Figs. 6 and 7 that there is one peak observed in all EEDFs measured at different conditions. This means that there is one group of electrons in all curves at different conditions. When the electron beam passes through the grid anode and moves toward the center, it makes a large number of ionizing collisions with gas atoms, producing a large number of secondary electrons. The secondary electrons are converged at the center, so they have enough time to be redistributed to form one group with a Maxwellian dis-

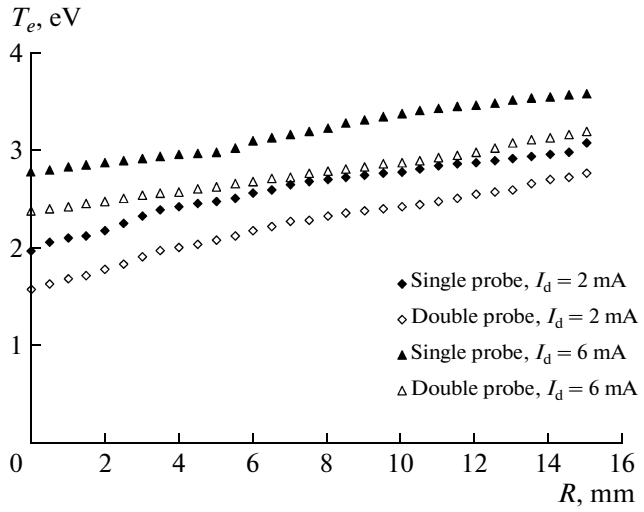

Fig. 8. Comparison between the radial profiles of the electron temperature measured using the single and double probes for 2 and 6 mA discharge currents at a constant nitrogen pressure of 3 mbar.

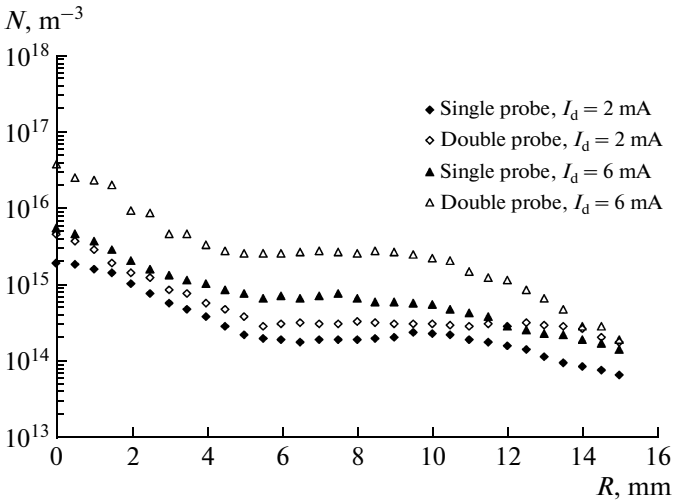

Fig. 9. Comparison between the radial profiles of the plasma density measured using the single and double probes for 2 and 6 mA discharge currents at a constant nitrogen pressure of 3 mbar.

tribution. It is seen from these figures that the distribution of electrons at all radial positions in the region from $R = 0$ to 15 mm is close to Maxwellian.

3.4. Measurements of the Electron Temperature and Plasma Density

The electron temperature can be determined from the EEDF curves. Thus, the electron temperature T_e equals twice of the average energy E_{av}, i.e., $T_e = 2E_{av}$ [28].

The electron temperature is also estimated from the I–V characteristic of the double probe using the following relation [29]:

$$T_e = \frac{\Delta V_p}{4}, \quad (5)$$

where ΔV_p is the potential difference between the two points of the saturation currents in the I–V characteristic of the double probe.

Figure 8 compares the radial distribution of the electron temperature for a dc cylindrical hollow-cathode discharge, obtained using the single and double probes. The measurements were carried out at a constant nitrogen pressure of 3 mbar and discharge currents of 2 and 6 mA. The electron temperature measured by the single probe varies from 2.8 eV at the center to 3.6 eV near the grid edge for the 2 mA discharge current and from 2 to 3.1 eV for the 6 mA discharge current. The electron temperature measured by the double probe varies from 2.4 eV at the center to 3.2 eV near the grid edge for the 2 mA discharge current and from 1.6 to 2.8 eV for the 6 mA discharge current.

It was found that the electron temperature increased with increasing discharge current and radial distance from the center toward the grid. This is because, when the electron beam passes through the grid anode, it has a high speed and hence a high energy. The electron beam makes a large number of inelastic collisions with gas atoms and loses its energy gradually as it moves along the radius toward the center. So, the electron temperature is high near the grid anode and decreases as the electrons move toward the center [30].

On the other hand, for a cylindrical single probe, the plasma ion density n_i [31] is

$$n_i = \frac{I_{is}}{0.4eA_p}\left(\frac{m_i}{2kT_e}\right)^{1/2}, \quad (6)$$

where m_i is the ion mass.

Figure 9 compares the radial distributions of the plasma density for a dc cylindrical hollow-cathode discharge, obtained using the single and double probes. The plasma density was measured at a gas pressure of 3 mbar and at discharge currents of 2 and 6 mA. For the single probe, the plasma density varies from 2×10^{15} m^{-3} at the center to 7×10^{13} m^{-3} near the grid edge for the 2 mA discharge current and from 5.9×10^{15} to 1.5×10^{14} m^{-3} for the 6 mA discharge current. For the double probe, the plasma density varies from 5×10^{15} m^{-3} at the center to 1.9×10^{14} m^{-3} near the grid edge for the 2 mA discharge current and from 3.9×10^{16} to 2×10^{14} m^{-3} for the 6 mA discharge current. One can see that the radial profiles of the plasma density obtained by the two methods have the same behavior.

Figure 9 shows that, as the electrons move radially from the grid until reaching the edge of the negative layer in the central region, the plasma density measured by the single and/or double probes first increases. Then, as the electrons move within this negative layer, the plasma density remains nearly constant. Finally, as the electrons move along the radius until reaching the center of the system, the plasma density increases again. Such behavior is explained as follows: after the electron beam passes through the grid anode toward the center, it produces a large number of secondary electrons due to ionizing collisions with neutral gas atoms. So, the plasma density increases as the electrons move toward the central negative layer. This layer reduces the number of electrons that move toward the center, and the secondary electrons, which lose their energy due to inelastic collisions with gas atoms, are trapped. As a result, in the central region, the electric field is very weak and the plasma density is nearly constant. After that, the passed electrons are converged from all directions and focused at the center; so, the plasma density increases as they move until reaching the center ($R = 0$) [32, 33].

4. CONCLUSIONS

In this paper, a dc cylindrical coaxial glow discharge with an inner grid anode has been studied. When the discharge voltage is applied between the two electrodes, breakdown occurs. The region between the two electrodes is seen dark, while a brightly glowing region forms inside the grid anode up to the center.

The I–V characteristic of the dc cylindrical glow discharge in nitrogen gas is similar to that of the normal glow discharge. Also, the discharge voltage increases with decreasing gas pressure at a constant discharge current. It is found that the normal glow discharge voltage decreases sharply in the pressure range between 0.5 and 3 mbar and decreases slowly at higher pressures due to an increase in the secondary ionization coefficient when the gas pressure increases.

The plasma potential has been determined using a single probe. The minimum potentials is observed at the negative layer due to the fraction of the electron beam that is decelerated in reaching the center and forming a negative layer at the back of the grid. This means that the number of electrons that pass the negative layer region becomes small; so, the electric field increases within that layer, still increasing as the center is approached. At the center, some of the passed electrons are converged, so the kinetic energy of these electrons increases and their potential decreases.

The theoretical EEDF has been calculated and compared with the experimental results obtained using the second derivative of the single probe characteristic at different radial positions (0, 5, 10, and 15 mm) and different discharge currents (2, 4, and 6 mA). It is shown that there is only one group of electrons with a Maxwellian distribution due to the secondary electrons that are converged at the center; so, they have enough time to be redistributed to form one group with a Maxwellian distribution.

The electron temperature measured by the single and double probes varies between 1.6 and 3.6 eV for different discharge currents and probe positions, while the plasma density varies between 3.9×10^{16} and 7×10^{13} m^{-3}. It is found that the electron temperature increases with increasing discharge current and radial distance between the center and the grid. The plasma density increases as the electrons move radially from the grid toward the negative layer, where it is nearly constant, because this region reduces the number of electrons that move toward the center and the secondary electrons, which lose their energy due to inelastic collisions, are trapped and their energy decreases.

REFERENCES

1. K. Yamauchi, Y. Takeuchi, Y. Ogino, et al., Electr. Eng. Jpn. **135** (2), 1 (2001).
2. Y. Gu and G. H. Miley, IEEE Trans. Plasma Sci. **28**, 331 (2000).
3. H. S. Uhm, E. H. Choi, and M. C. Choi, Appl. Phys. Lett. **79**, 913 (2001).
4. K. Rozsa, M. Janossy, L. Csillag, and J. Bergou, Phys. Lett. A **63**, 231 (1977).
5. K. Rozsa, M. Janossy, J. Bergou, and L. Csillag, Opt. Commun. **23**, 15 (1977).
6. K. A. Peard, Z. Donko, K. Rozsa, et al., IEEE J. Quant. Electron. **30**, 2157 (1994).
7. K. Rozsa, M. Janossy, L. Csillag, and J. Bergou, Opt. Commun. **23**, 162 (1977).
8. T. Iijima, Jpn. J. Appl. Phys. **20**, L470 (1981).
9. T. Iijima, Jpn. J. Appl. Phys. **21**, L597 (1982).
10. K. Fujii, Jpn. J. Appl. Phys. **14**, 1339 (1975).
11. K. Fujii, S. Miyazawa, S. Takano, and T. Oikawa, Jpn. J. Appl. Phys. **18**, 803 (1979).
12. K. Fujii, Jpn. J. Appl. Phys. **16**, 1081 (1977).
13. D. C. Gerstenberger, R. Solanki, and G. J. Collins, IEEE J. Quant. Electron. **16**, 820 (1980).
14. A. Grill, *Cold Plasma in Materials Fabrication* (IEEE, New York, 1993).
15. M. A. Lieberman and A. J. Lichtenberg, *Principles of Plasma Discharges and Materials Processing* (Wiley, New York, 1994).
16. S. Lee, in *Proceedings of the First Tropical College on Applied Physics "Laser and Plasma Technology,"* Kuala Lumpur, 1985, p. 421.
17. G. Francis, in *Handbuch der Physik*, Ed by S. Flügge (Springer-Verlag, Berlin, 1956), Vol. 22, p. 53.
18. A. von Engel, *Electric Plasmas: Their Nature and Uses* (Taylor & Francis, New York, 1983).
19. A. A. Garamoon, A. Samir, F. F. Elakshar, and E. F. Kotop, Plasma Sources Sci. Technol. **12**, 417 (2003).
20. S. E. Coe, J. A. Stocks, and A. J. Tambini, J. Phys. D **26**, 1203 (1993).

21. E. Passoth, P. Kudrna, C. Csambal, et al., J. Phys. D **30**, 1763 (1997).
22. V. I. Kolobov and L. D. Tsendin, Phys. Rev. **46**, 7837 (1992).
23. W. Jiang, K. Woolverton, and J. Dickens, IEEE Trans. Plasma Sci. **27**, 1538 (1999).
24. V. A. Godyak, R. B. Piejak, and B. M. Alexandrovich, J. Appl. Phys. **73**, 3657 (1993).
25. H. Singh and D. B. Graves, J. Appl. Phys. **87**, 4098 (2000).
26. V. A. Godyak, R. B. Piejak, and B. M. Alexandrovich, Plasma Sources Sci. Technol. **1**, 36 (1992).
27. F. F. El-Akshar, M. A. Hassouba, and A. A. Grar-amoon, Fizika A **9**, 177 (2000).
28. J. R. Roth, *Industrial Plasma Engineering* (IOP, Bristol, 2001), Vol. 1.
29. M. Konuma, *Film Deposition by Plasma Technology* (Springer-Verlag, New York, 1992).
30. A. M. Shager, A. T. Sroor, H. A. El Tayeb, et al., Z. Naturforsch. A **63**, 412 (2008).
31. R. Hippler, S. Pfau, M. Schmidt, and K. H. Schoen-bach, *Low Temperature Plasma Physics* (Wiley, Berlin, 2001).
32. M. A. Saudy, A. I. Eatah, and M. M. Masoud, Fizika A **14**, 225 (2005).
33. K. Kato, S. Lizuka, and N. Sato, Appl. Phys. Lett. **65**, 816 (1994).